Sensitivity assessment of a novel earth fault location method with optimally placed distributed measurements for MV networks

Alexandre Bach, Trung Dung Le, Marc Petit

Received: 6 October 2022 | Revised: 16 November 2022 | Accepted: 13 December 2022

IET Generation, Transmission & Distribution

DOI: 10.1049/gtd2.12740

The Institution of Engineering and Technology WILEY

ORIGINAL RESEARCH

Sensitivity assessment of a novel earth fault location method with optimally placed distributed measurements for MV networks

Alexandre Bach | **Trung Dung Le** | **Marc Petit**

Group of Electrical Engineering of Paris, CNRS, CentraleSupelec, Paris-Saclay and Sorbonne Universities, Plateau de Moulon, France

Correspondence
Alexandre Bach, Group of Electrical Engineering of Paris, CNRS, CentraleSupelec, Paris-Saclay and Sorbonne Universities, Plateau de Moulon, 91192 Gif sur Yvette, France.
Email: alexandre.bach@centralesupelec.fr

Abstract

This paper extends the study of a zero-sequence impedance-based fault location method (FLM) designed for medium voltage (MV) distribution feeders whose principle has been presented in a previous work Bach et al. This method is able to locate any type of earth fault with any type of neutral grounding inside a convex set of nodes forming the solution area. The total length of the lines inside this area is statistically computable a priori and depends only on the number and location of additional voltage measurements deployed on some remote end secondary substations. To be efficiently applied to the most challenging rural feeders presenting a lot of ramifications, simulations have shown a need for synchronized measurements, such as the ones obtained using phasor measurement units. Besides, this paper addresses the coupling potential of this method with more traditional ones such as Takagi-based FLMs to enhance the performances of both, solving the multiple estimation problem while potentially locating the fault within one node. Finally, an extensive sensitivity analysis has been carried out, showing a good robustness with respect to impedance estimation errors or fault impedance values while showing the need for synchronization, especially on some remote measurement locations.

1 | INTRODUCTION

Fault detection and location are critical for a distribution system operator (DSO). Indeed, the system restoration time, and by such the value of lost load, depends on the time in which maintenance teams are able to reach the fault and repair the faulty component so that nominal configuration can be restored. That is why having a fault location algorithm at the distribution level highly increases the reliability indices of the grid, such as SAIDI or SAIFI [1], with respect to visual inspection by teams going through the whole feeder. Usually, MV distribution feeders are operated with a radial topology with the only instrumented nodes being located at the primary substation, where currents on all feeders and busbar voltage are measured. With the increasing stress faced at the distribution level, there is a need for smarter grids, in which more nodes, especially some secondary substations, would be instrumented, as some DSOs already experimented. Indeed, in the project [2], 130 secondary substations from six feeders have been instrumented.

There are two main types of FLMs proposed in the literature. First, the ones which study the fundamental component of voltages and currents are known as impedance-based methods [3, 4, 5]. They are said to be cost-efficient but face the problem of multiple location estimation on radial grids with a single-end measurement [6, 7]. Since the usual case is that only the primary substation is instrumented, it is not possible to differentiate the apparent impedance of two nodes located on two different ramifications—which can be far away from each other—but at the same electrical distance of the primary substation. Second, transient-based methods have been deployed at the transmission level and rely mainly on the measurement or estimation of the propagating time of the wave induced by the step change in voltage at the fault location when the fault is triggered. Different methods have been proposed based on direct propagation time measurement [8, 9], time-reversal similarity [10, 11], wavelets [12] and others to obtain the fault location. These methods are said to be more accurate at the expense of the need of devices with very high sampling frequencies to be

able to see transients with such high propagation speed. Given that there are still few devices compliant with this requirement deployed at the distribution level, this paper chose to present an impedance-based FLM which tries to solve the multiple estimation problem by adding a limited number of measurements using the current generation of sensors usually used by DSOs regarding the sampling frequency. Besides, machine learning techniques are proposed to solve the fault location problem [13, 14, 15].

Solving the multiple estimation problem can be achieved with the installation of additional measurements on a feeder [16, 17]. In the literature, the most popular method to obtain the number and location of needed additional measurements is based on the observability of the voltage on all the nodes of the feeder and is called the "1-bus spaced placement strategy" [18]. While respecting this criterion provides the DSO with enough information to also perform accurate state and/or parameters estimation of the grid, it comes at the cost of a very high number of measurement nodes [19]: up to 35% of the nodes needs to be instrumented depending on the complexity of the topology of the feeder. The authors in[20] proposed a fault location observability formulation for transmission grids. This method would also lead to a very high number of additional measurements to guarantee that all faults are uniquely located, which is not a need at the distribution level. Implementing those placement methods would need an investment that is not in DSOs range given the added value of fault location in terms of exploitation of these grids, especially considering long rural and ramified feeders where hundreds of sensors would be needed for each one of them.

When performing voltage sag estimation along a faulty transmission line from both ends, there is an equality of the two voltage estimates on the fault position [21]. If we want to apply such a method on a MV feeder, a DSO would need to measure the value of load current at every injection node, which is needed to solve the multiple estimations with most of the impedance-based FLMs. This would greatly reduce the deployability of the method since a DSO usually does not dispose of the needed measurements, and the installation of such a high number of them is not economically viable. To overcome this issue, [22] proposed an FLM based on the same principle using the negative sequence components under the hypothesis that the value of load current can be neglected in the negative sequence. This hypothesis seems too strong when compared to real-field data. A negative-to-positive sequence current ratio has been measured ranging up to 39.6% in the healthy feeders which are neighboring the faulty one. Under the hypothesis that the loads in the faulty feeders should behave the same way as the loads in the healthy feeders, the hypothesis made by [22] seems too strong to be applied for every case at the distribution level even though the negative sequence current can sometimes be neglected in the faulty feeder.

A method based on the interpolation of the voltage profile before and after the faulty node has been proposed in [23], which needs four measurement nodes for each considered path and which is not robust to load current values and not well suited for heterogenous feeders, such as the ones encountered in rural areas.

An FLM using incremental values and two synchronized measurements to estimate the fault current value is shown in [24], which enables them to obtain the fault location providing that every node at remote ends of the feeder is equipped with a voltage measurement, which is similar to [25]. While this condition is easily achievable on urban weakly ramified feeders, it seems economically difficult to achieve in rural areas. When dealing with long and ramified feeders, some end nodes have been disregarded without quantification of the impact of the missing measurements on the locating performances of the proposed method.

Moreover, the differences of zero-sequence line impedance values due to misestimation of earth resistivity, which [22] seem too important at the transmission level, are smaller when focusing on distribution grids. This increases the global confidence in the zero-sequence impedance values stored in DSO databases. Most of the French MV feeders are exploited with transformers that have one delta-coupled winding, thus preventing zero-sequence currents from going out of the MV level. That is why knowing line impedances and zero-sequence voltage and current at the primary substation is enough to compute zero-sequence voltage and current in all the nodes of the feeder when sound, without a need for load current values. That is why the fault location algorithm, whose principle is presented in [26], is based on zero-sequence components. It exhibits a convex set of nodes around the faulty one defining a solution area whose statistical size can be computed a priori in function of the number and location of additional measurements.

The original contribution of this paper resides first in the theoretical demonstration of the fact that only remote end substations should be regarded as viable candidates for additional measurement placement for this FLM (in Section 2.2). Second, the impact of the number of additional measurements on the length of the solution area in function of the ramification index of the feeder is presented. This study has been carried out considering reconstructed realistic and long feeders which have a more complex and closer-to-reality topology than most of the benchmark feeders commonly used in the literature (in Sections 3.1, 3.2 and 3.3). Moreover, first results regarding the coupling potential with another impedance-based FLM are presented (in Section 3.4). Finally, an extensive sensitivity analysis has been carried out focusing on the impact of fault impedance value, misestimation of line impedance values and location and synchronization of additional measurements (in Section 4). The impact of the combination of all these sources of errors on the locating performance is not yet well described in the literature.

This paper is structured as follows: Section 2 presents an overview of the developed fault location and optimal measurement placement methods. Then, Section 3 reports the results with an exhibition of the opportunity for coupling with other FLMs. Section 4 shows the sensitivity analysis of the location algorithm with respect to impedance values errors, fault position feeder ramification index, and measurement synchronization.

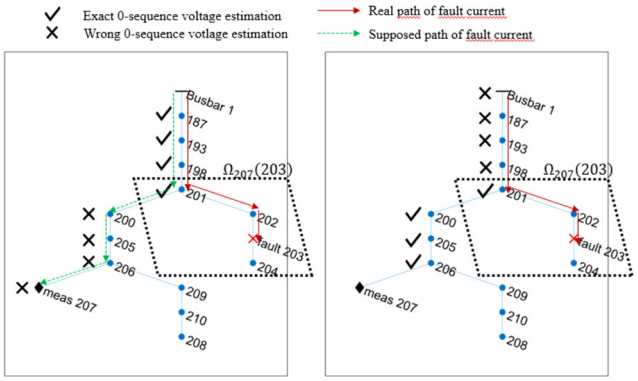

FIGURE 1 Example of the Top-Down (left) and Bottom-Up (right) voltage estimation between busbar and node 207

2 | PRESENTATION OF THE METHODS

2.1 | Fault location method

The presented FLM relies on the comparison of two zero-sequence voltage estimate sets, the Top-Down estimation and the Bottom-Up estimation, along a path between the busbar and an additional measurement node. The methodology has been presented in [26] and is recapitulated here. As in DSO databases, a PI lumped-parameters model is considered for the lines, including serial resistance and reactance, and parallel capacitance. Figure 1 exemplifies the method's principle on one of the simplest reconstructed feeders described in the next part. The fault—which could be any type of earth fault—is occurring at node 203. For this example, we considered the path between the busbar and the first measurement node: node 207. During the Top-Down estimation, the faulty current measured at the busbar is used for the computation of the voltage drops along the path (node 1 to node 207 in Figure 1), and not only for the nodes along the actual fault current path (node 1 to node 201). So, the voltage drops computed match the real voltage drops induced by the fault for nodes in the fault path while the computed voltage drops are inaccurate for the other nodes (node 200 to node 207) through which only a capacitive current is flowing. Symmetrically, during the Bottom-Up estimation process, only the capacitive current is considered since the fault position is not known and no zero-sequence current can be measured in Delta-coupled windings in the secondary substation. This leads to erroneous voltage drops estimations on the nodes located in the actual fault current path (node 1 to node 198), where there is a faulty current which is not being taken into account, while the voltage drops estimates will be accurate for the other nodes (node 207 to node 201), where only the capacitive current is flowing.

As a result, for a given path from the primary substation to a measurement node, the two sets of voltage estimates are equal on the node which is the nearest to the fault while on the path between the two considered measurements. It is called the projection node here. To obtain such a node, the values of the two zero-sequence voltages estimates are compared. If the measurements are synchronized together, as when using PMUs, the difference of the phasors, obtained here using discrete Fourier transform (DFT)-based synchrophasor estimators, can be performed while only the difference of magnitudes is computable when using unsynchronized measurements.

Once the projection node is obtained, the lateral branch is defined as the set of nodes being downstream to the projection node but outside the path under study. In Figure 1, the lateral branch of node 201 with respect to the path from 1 to 207 is the set of nodes $\Omega_{207}(203) = \{201, 202, 203, 204\}$. If the closest node to a fault position is any of these nodes, the FLM would give the same answer, that is, the projection node is node 201 and it is not possible to locate the fault more precisely inside this set without adding another measurement. We chose to name the length of the upstream branch of node k as L_k, the interior of $\Omega_{207}(203)$ as $Int[\Omega_{207}(203)]$ and the boundary of $\Omega_{207}(203)$ as $\partial\Omega_{207}(203)$, such as $\Omega_{207}(203) = Int[\Omega_{207}(203)] \cup \partial\Omega_{207}(203)$. Then, in this example a fault occurring along the branches inside the interior of solution area—that is, $L_{202}, L_{203}, L_{204}$—and along the closest half of the branches at the boundary $\partial\Omega_{207}(203)$, that is, L_{201} and L_{200} would be located in the same area $\Omega_{207}(203)$:

$$\Omega_{sol}^{M}(j) = \bigcap_{i=1}^{M} \Omega_{m_i}(j). \tag{1}$$

In the case of one or more misfunctioning measurements or even a wrong estimation of the projection node, the solution area defined by (1) would be too restrictive and might not include the faulty node. That is why there is a need to define solution areas of increasing likelihood of fault location (2). We chose to exhibit the set Ω_{sol}^{k} of nodes which are included k times in one of the solution areas. For each node n of the grid, we count this number of times $N_\Omega(n) \in [\![0..M]\!]$. These solution areas are represented in the next parts of the paper:

$$\Omega_{sol}^{k}(j) = \{n : N_\Omega(n) \in [\![k..M]\!]\}. \tag{2}$$

2.2 | Optimal measurement placement

Usually, the performance of a location algorithm is quantified by the distance between the true fault location and the estimated one. Since the presented FLM cannot distinguish the nodes inside of the solution area—that is, Ω_{sol}^{M} for M additional measurements considering the best-case scenario—this performance index cannot be used. So, we propose a new performance index suited for the developed FLM. The locating performance can be considered as high as the total length of the lines inside and at the boundaries of the solution area is small. By this way, it is correlated to the time required for a maintenance team to travel across the solution area in search for the fault. To obtain the best performances of the FLM, there is a need for an optimal placement of the M wanted additional measurements. For this purpose, we define the probability of a fault to occur in a node j of the feeder as $FP(j)$. The general expression of the total length of the lines in a given solution area for a given

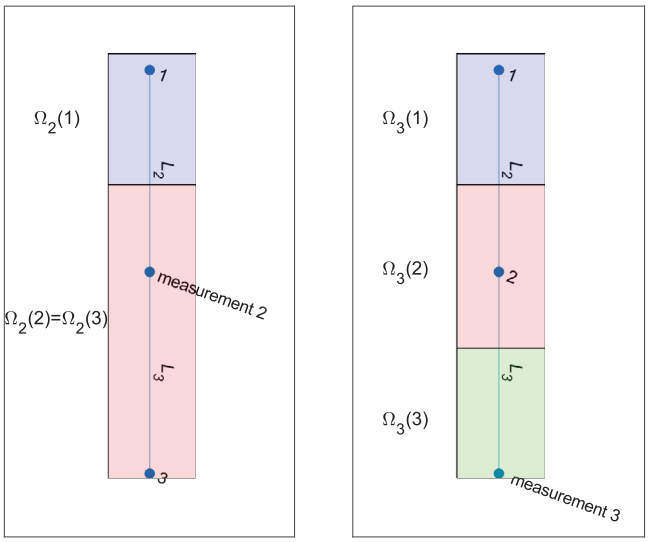

FIGURE 2 Comparison of the possible solution areas of the FLM for a 3-nodes feeder with measurement at node 2 and 3

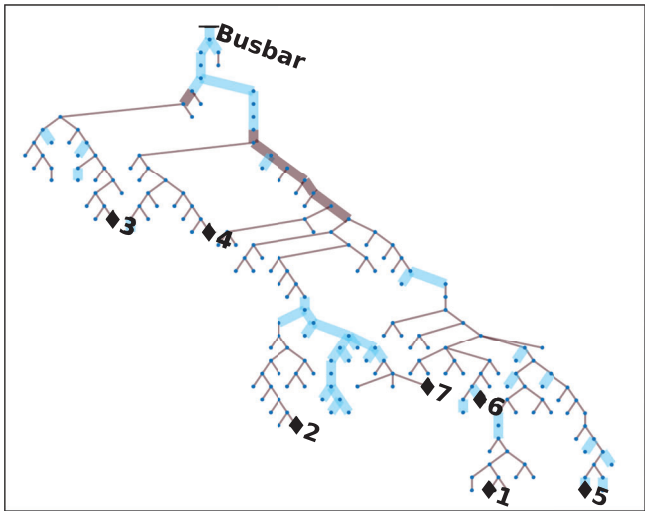

FIGURE 3 Optimal placement considering the fault PDF with measurement priority placement (diamond nodes)

set of nodes X_M where additional measurements are installed is given by (3), and it is equal in the example of Figure 1 to $L_{sol}^{X_1=\{207\}}(203) = L_{202} + L_{203} + L_{204} + \frac{L_{201}}{2} + \frac{L_{200}}{2}$. There is a need to solve a combinatorial optimization problem to find the set of M additional measurements X_M so that the expectancy $\mathbb{E}[L_{sol}^{X_M}]$, as introduced by (4), is minimized (5):

$$L_{sol}^{X_M}(j) = \sum_{x \in \partial\Omega_{sol}^{M}(j)} \frac{L(x)}{2} + \sum_{k \in Int[\Omega_{sol}^{M}(j)]} L(k), \tag{3}$$

$$\mathbb{E}\left[L_{sol}^{X_M}\right] = \sum_{j \in nodes} L_{sol}^{X_M}(j) FP(j), \tag{4}$$

$$\widehat{X_M} = \arg\min_{X_M} \mathbb{E}\left[L_{sol}^{X_M}\right]. \tag{5}$$

To obtain $\widehat{X_M}$, an iterative and exhaustive method is employed. The optimal placement algorithm iteratively searches for the best node to add a measurement on considering $X_i, i \in [\![0..M-1]\!]$ already present measurements. This iterative approach would enable a DSO to optimally place a set of additional measurements and later optimally place some more. Besides, this approach reduces the complexity of the combinatorial optimization problem.

A branch-and-bound strategy has been adopted to reduce the size of possible candidates for measurement placement. It is possible to consider only the most remote end nodes as candidates for the measurement placement instead of all nodes since they provide us with better information than their upstream nodes. To demonstrate this, let us consider a 3-node straight-line feeder with the busbar as node 1, and nodes 2 and 3 being at distance L_2 and $L_2 + L_3$ from node 1, respectively (Figure 2). Then, adding an additional measurement at node 2 would give the possibility to differentiate two solution areas composed of $\Omega_2(1) = \{1\}$ or $\Omega_2(2) = \Omega_2(3) = \{2, 3\}$, as shown in Figure 2, which leads to the statistical expectation of the solution area shown in (6). However, adding the additional measurement to the most remote node 3 enables the discrimination of three solution areas $\Omega_3(1) = \{1\}$ or $\Omega_3(2) = \{2\}$ or $\Omega_3(3) = \{3\}$, which gives an expectation of the length of the solution area shown in (7):

$$\mathbb{E}\left[L_{sol}^{X_1=\{2\}}\right] = \frac{FP(1).L_2}{2} + (FP(2) + FP(3)).\left(\frac{L_2}{2} + L_3\right), \tag{6}$$

$$\mathbb{E}[L_{sol}^{X_1=\{3\}}] = \frac{FP(1).L_2}{2} + FP(2).\frac{L_2 + L_3}{2} + \frac{FP(3).L_3}{2}. \tag{7}$$

It appears that $\mathbb{E}[L_{sol}^{X_1=\{2\}}] \geq \mathbb{E}[L_{sol}^{X_1=\{3\}}]$. So, if a given node has a downstream node, positioning the additional measurement in the downstream node provides us at least with the same information as with the upstream node but more if a fault occurs downstream. Given that, we consider only the most remote (extremity) nodes of the feeder as potential candidates for measurement placement. From this, we reduce the size of the variable vector from all secondary substation nodes to all extremity substation nodes. We are able to iteratively test all the remote nodes as possible candidates selecting the best at each iteration, which gives us the priority of placement of additional measurement shown in Figure 3.

3 | LOCATING POTENTIAL

3.1 | Use case

The topology of most of the MV benchmark feeders is too simple to be representative of the complex feeders, such as the ones found in rural areas. That is why there is a need to test the behaviour of the presented FLM on a set of feeders with ramified and long ones, which are the worst-case scenarios for impedance-based FLMs.

To achieve this objective, we used 20 realistic feeder models from a French HV/MV substation that have been built using an open data database from Enedis [27]. The FLM has been simulated on the reconstructed feeders using MATLAB/Simulink running on a PC equipped with an Intel(R) Core(TM) i7-10700 CPU and 32 GB of RAM with compensated neutral grounding, which is the most challenging case for FLMs due to the low value of fault current. The DFT is used to estimate the phasors at each measurement node in steady state with compensation of the possible offset of the measurement devices with mean subtraction. Then, the Fortescue transform is applied to obtain the zero-sequence components. The longest and most ramified out of the 20 reconstructed ones, which is shown in Figure 3, has been chosen to be exhibited here as it is the worst-case scenario. It is a 211-node feeder with a total length $L_{tot} = 75.05$,km. Overhead lines (OHLs) are shown using red color and underground cables are represented using a light blue color. High section lines (with $r_d \leq 0.4\,\Omega.km^{-}1$ meaning bigger than around $80mm^2$) are represented widened whereas small section lines are thinner. A ramification index is defined in (8) and enables us to describe the complexity of the topology with a single index, as the ratio between total length of the feeder's lines and distance of the farthest (most remote) node. By comparison, the CIGRE MV benchmark distribution network, which is one of the most used benchmark network, has a ramification index of $ram = 1.39$ only.

$$ram = \frac{L_{tot}}{d_{remote}} = 3.22 \tag{8}$$

We simulated the installation of the four most needed measurements obtained from the optimal placement method presented in the previous part. It corresponds to a DSO who would want that the statistical length of the solution area $\mathbb{E}[L_{sol}]$ is less than 4% of the total length of the feeder, as shown in the 20th and last column of Figure 5. An SLG fault on phase A on the node 1043 called the faulty node has been simulated. A fault resistance $R_f = 150\,\Omega$ is considered. The faulty node is located at distance $d_{fault} = 18.9\,km = 0.81 \times d_{remote}$ from the busbar. To represent the reality of the repartition of fault occurrences, we took into account the fact that underground cables are far less subjected to faults than OHLs, as shown in [28] presenting the 1991 statistics in France. The fault probability was at that time 13 times higher on OHLs than on underground cables. That is why a 10 times higher fault probability on OHLs has been chosen. The faulty node is a node with high fault probability while being one of the worst-case scenarios for this set of additional measurements.

3.2 | Measurement placement priorities

Figure 3 presents the topology of the considered feeder. The priority order of placement of measurements is shown with the black nodes having a label, so that a DSO who would want to equip M (M up to seven in Figure 3) secondary substations with additional voltage measurements should equip the ones labelled from 1 to M. As expected, the first needed measurement location is one of the farthest away substations from the busbar, since it provides the longest path of nodes, forming the main artery. Then, the other substations on which putting an additional measurement would be efficient are located at the end of the longest lateral branches to this main artery. For example, we can see that the second most needed additional measurement is at the end of a long OHL branch since it presents the highest fault probability, meaning that a DSO can save some measurement devices where there is a lot of underground cables (since they have a lower fault probability) or can deploy them at the end of another branch where they should prove more useful. This means that to ensure that the placement of the wanted additional measurements reaches its maximum efficiency with this FLM on a given feeder, a DSO would need to provide the algorithm with local fault probabilities at the node level. For example, a higher fault probability could be given to nodes located inside a forest.

The developed FLM is able to cover a high part of a complex and highly ramified feeder with a rather small number of additional measurements—placed at some remote substations—compared to the methods proposed in the literature. The optimization of measurement placement could enable DSO to perform fault location with a limited number of added measurements, which means for a limited investment cost. We are able to locate faults (i) at the node scale when occurring around a node located on one of the paths between the busbar and an additional measurement, (ii) while having a solution area with a set of nodes when faults occur on the lateral branches.

3.3 | Results-fault location and length of solution areas

A statistical study of the expectancy of the length of the solution area across all nodes on this reconstructed feeder has been carried out. Figure 4 presents the evolution of $\mathbb{E}[L_{sol}]$ and the worst-case length of solution area L_{sol}^{max} with the number of additional measurements placed on the considered feeder. It appears that the impact of adding more measurement is logarithmic in the sense that the first ones reduce $\mathbb{E}[L_{sol}]$ more than the next ones. We can see that adding a second additional measurement divides the statistical length of the solution area by more than two whereas the third measurement only yields a factor of 1.3. Moreover, the proposed locating method is able to locate any earth fault within an area whose size is statistically less than 2% of the length of the feeder with only six additional measurements on this feeder which is the most challenging on this HV/MV substation. In order to see the locating potential in different feeders, we computed the minimum number of additional measurements needed to ensure that $\mathbb{E}[L_{sol}] \leq x\%$ on all 20 reconstructed feeders, sorted by their ramification index. The result is presented in Figure 5. The proposed FLM is particularly well suited for long and ramified rural feeders, on which it can locate faults with one measurement within a 12%-long area (except for one feeder) and within

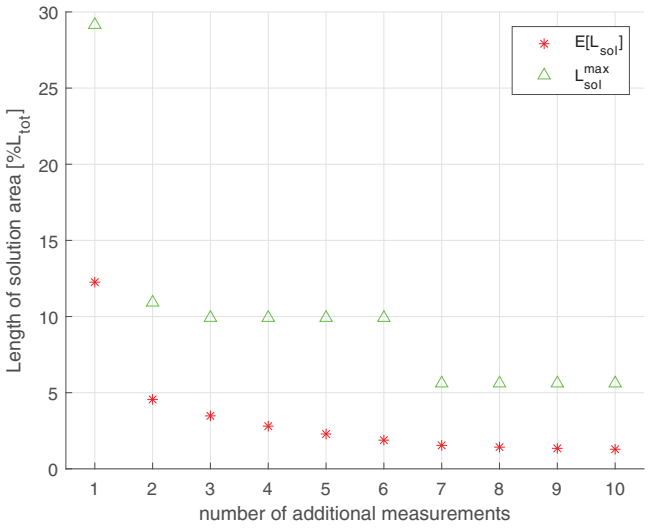

FIGURE 4 Expected and maximal value of L_{sol} for the considered 20th feeder (diamond nodes)

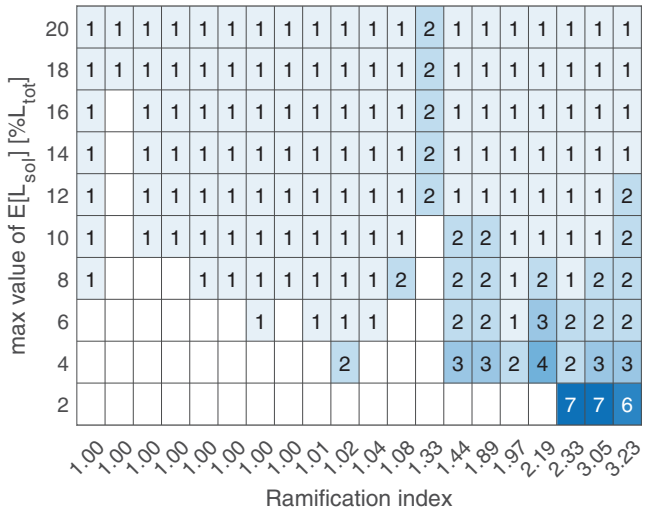

FIGURE 5 Minimum number of additional measurements needed to obtain a locating performance across the 20 reconstructed feeders ordered by ramification in columns

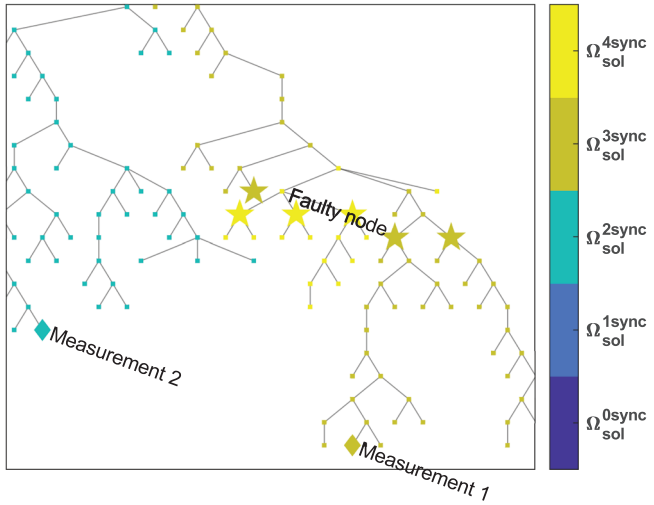

FIGURE 6 Comparison of two FLM results on the same fault with colouration by result of the presented FLM and stars for results of the Takagi method

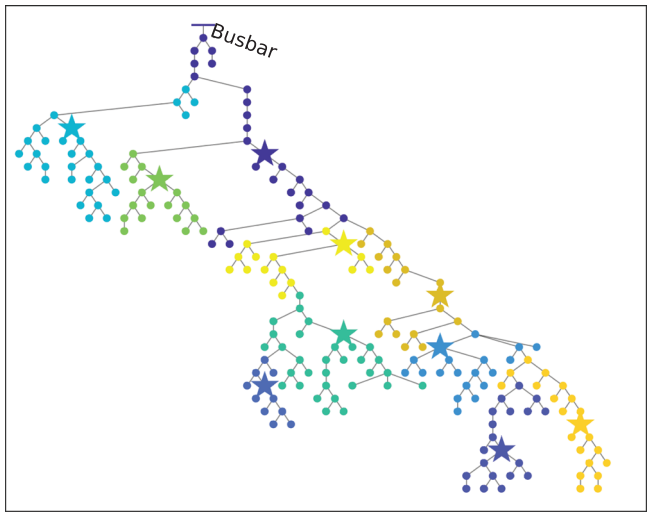

FIGURE 7 Clusters (colours) and the 10 fault positions tested (pentagram nodes)

a 6%-long area with a second measurement (except for one feeder). This represents an area containing less than 4.5, km of lines for the longest feeder with two measurements. On the lowly ramified feeders ($ram \approx 1$) such as the ones encountered in urban areas, the presented FLM cannot distinguish faults more precisely than between two nodes, which can be limiting when dealing with feeders with relatively long lines and spaced nodes. It should be said that, while its relative value can be high ($\mathbb{E}[L_{sol}] = 18\%$ on the second feeder), the absolute value of the length of the solution areas is small ($\mathbb{E}[L_{sol}] = 0.8\,km$). An extrapolation of the two voltage estimates on virtual nodes along the lines around the projection node could be performed to enhance the locating performances on this type of feeders.

3.4 | Comparison with other FLMs and coupling potential

The behaviour of this FLM suggests a high opportunity for coupling with other impedance-based ones. For example, using Takagi-based FLM [6], we often obtain a set of nodes with close electrical distance to the busbar while being geographically far away from each other since they might be located on different branches. With the presented FLM, a convex set of nodes around the fault is obtained. So, coupling these two algorithms can enhance the performance of both since we can disregard some of the solution nodes of the Takagi method and we can obtain an indication of the most probable nodes inside of the solution area of the presented method. Figure 6 presents the results of both methods on the simulated A-G fault with $R_f = 150\,\Omega$ with compensated neutral grounding and

the four additional measurements. Only the neighbouring nodes of the faulty ones are displayed to better see the results. The nodes are coloured in function of the likelihood of fault location k computed by the presented FLM, and stars have been put on the nodes which are solutions of the Takagi-based algorithm. We get six potential fault locations using the Takagi-based algorithm while three of them are inside the most likely fault location area of the presented FLM Ω^4_{sol} and three other nodes inside Ω^3_{sol}. As shown, the coupling of the presented algorithm with another impedance-based one can enhance the results of both. The confidence in the results is increased since half the solutions of the Takagi-based FLM are located inside the most likely solution area. Moreover, the size and geographical extent of the solution can be reduced by disregarding the three solutions inside Ω^3_{sol} and only keeping the nodes inside Ω^4_{sol} neighbouring the three selected solutions of the Takagi-based method.

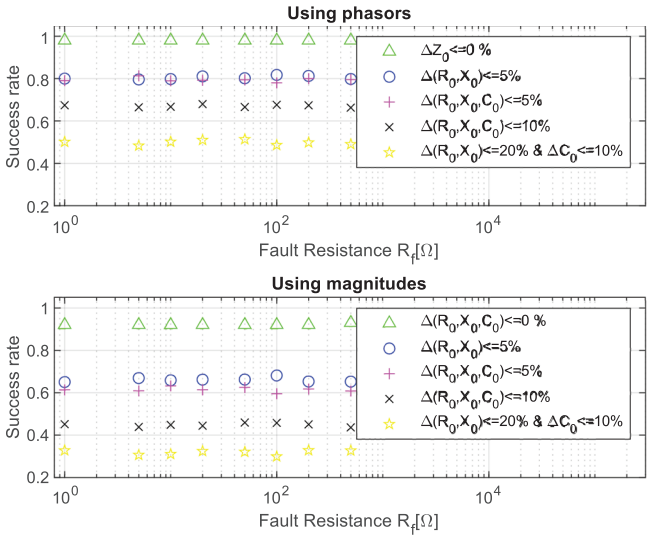

FIGURE 8 Success rate with and w/o synchronization in function of the fault resistance and line impedance values uncertainties-results for the feeder 20 shown in Figure 3

4 | SENSITIVITY ANALYSIS

4.1 | Presentation of the methodology

In order to assess the possibility of deployment of this FLM in real field, there is a need to assess the sensitivity to different parameters such as errors in line impedance values or measurement errors among others. That is why a Monte-Carlo simulation has been performed. First, we simulated 10 faults on the 20th and most challenging feeder presented in Figure 3. The fault locations have been chosen using a clustering algorithm based on K-means so that we get 10 convex clusters with a minimized variance of the fault probability. In each cluster, representing an equivalent fault probability, the barycenter has been chosen to be the fault location so that the way faults are placed is deterministic and all parts of the feeder are explored. The result is presented in Figure 7. The considered variable parameters are the fault resistance with eight considered possible values ranging in $R_f \in [1, 500]\,\Omega$. The limit of 500 Ω has been chosen taking into account that there is less than 10 % of the faults with higher resistance than 150 Ω according to the statistics presented in [28]. Moreover, with higher fault resistances, the fault detection cannot be assured, especially in the considered compensated neutral grounding. The line impedance value errors are chosen uniformly distributed with $\Delta(R_0, X_0) \in [-20\%, +20\%]$ and $\Delta C_0 \in [-10\%, +10\%]$, which seems a reasonable error since real fault data obtained from Enedis enabled us to compute a statistical zero-sequence capacitance error at the feeder level of 6%. When R_0, X_0, C_0 are considered simultaneously with errors, we refer to their variation interval as $\Delta(R_0, X_0, C_0)$. A design of experiments with six combinations of impedance errors has been selected for presentation here. For each of the combination, $N_{MC} = 50$ simulations have been performed and the mean success rate (SR) of each measurement has been stored. This means that on this feeder, a total of 24,000 simulations have been performed. The success rate is defined as the rate for which a given measurement successfully finds the theoretical projection node associated with the fault location. For the study of the impact of measurement position, the top 10 priority measurements have been considered. Second, in order to study the influence of the feeder topology and ramification on the performances of the FLM, one fault randomly positioned in each feeder of the 20 feeders has been simulated. The fault impedance is constant $R_f = 150\,\Omega$ and the design of experiments is the same with six combinations of line impedance errors. On each feeder, we tested the fault location method considering the top 10 (upper value) most priority additional measurement locations, leading to a total of 87 measurement positions across the 20 feeders. For each combination, $N_{MC} = 50$ fault simulations have been performed, and we analyzed the mean of the SR, which is set to 1 for each experiment if a measurement locates exactly the projection node and 0 otherwise. A total of 48,000 fault configurations have been simulated across the 20 feeders.

4.2 | Influence of line and fault impedances

The average success rate is presented in Figure 8 in function of the maximum errors committed on the impedance line values in the design of the experiments. As shown, the fault resistance value has no influence on the performances of the method since all the curves are flat. The proposed FLM performs as expected even with high impedance faults for all the tested values up to $R_f = 500\,\Omega$. Besides, we observe that the second case (blue circles) and the third case (pink crosses) are quite the same. Given the fact that the only difference is the uncertainty on the capacitance with $\Delta C_0 \leq 5\%$ in the third case, we can say that errors in the line capacitance estimation have a small impact on the behaviour of the algorithm. This assumption is verified on all simulated faults on the 20 reconstructed feeders. The success rate of the 87 possible additional measurements across the 20 feeders for $R_f = 150\,\Omega$ has been computed in function of the

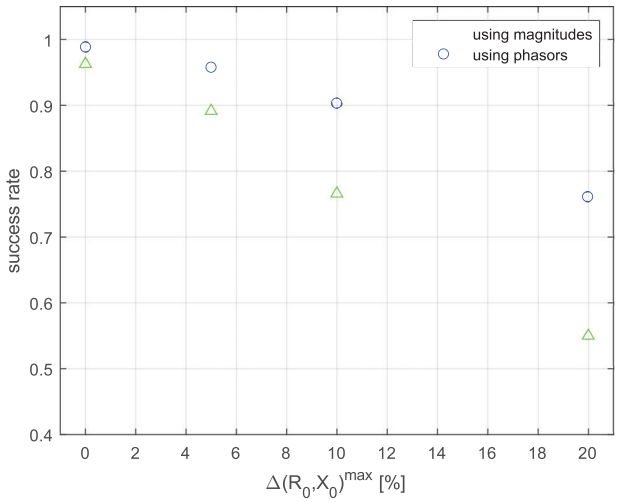

FIGURE 9 Average success rate on the 20 feeders in function of line impedance errors

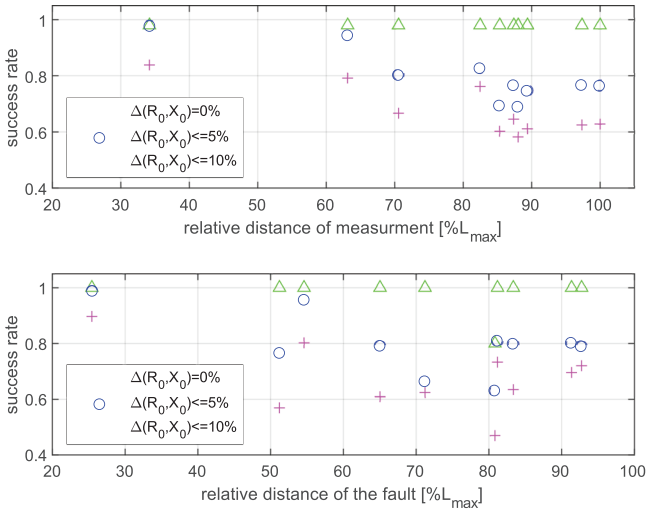

FIGURE 10 Influence of the fault and measurement positions

errors in line impedance estimation, as shown in Figure 9. We observe that the errors in capacitance value estimation have a negligible impact on the performance of the FLM overall. Moreover, we observe a linear decrease in the success rate (SR) with the uncertainties on R_0 and X_0. A linear regression of the curves is given in (9) and (10):

$$\frac{\Delta SR}{\Delta(R_0, X_0)}|_{phasors} = -1.1, \tag{9}$$

$$\frac{\Delta SR}{\Delta(R_0, X_0)}|_{magnitudes} = -2.2. \tag{10}$$

Using synchronized measurement reduces the impact of line series impedance estimation errors by a factor of 2. For example, to have a 95% success rate, a DSO would need to know the series line impedance parameters with errors inferior to $\Delta(R_0, X_0)^{max}|_{95\%} = 4.5\%$ if synchronized measurements are installed. When the phase information is not available, the line impedance errors should not be greater than $\Delta(R_0, X_0)^{max}|_{95\%} = 2.3\%$. Besides, [26] has shown that only using magnitudes can lead to misestimation of the projection even when all parameters are known, which shows that the need for synchronization is reinforced even further when considering line impedance errors in DSO databases. Overall, the proposed FLM can be called robust to impedance estimation errors to an extent large enough so that it can be deployed in real field using values stored in DSO databases.

4.3 | Influence of the position of the measurements and faults

On the simulated 10 fault positions and considering the fault location algorithm with the top 10 priority additional measurements, we observed that the more the measurement is far away from the busbar, the more the success rate in estimating the projection node decreases. However, when looking at the evolution of the success rate in function of the position of the fault, we observed that the most difficult to locate without errors are the ones located at the ends of the long branches lateral to the main artery, which are often located between 50% and 80% of the maximum distance to the busbar. This explains the decrease and then increase of the success rate in function of the position of the fault in Figure 10

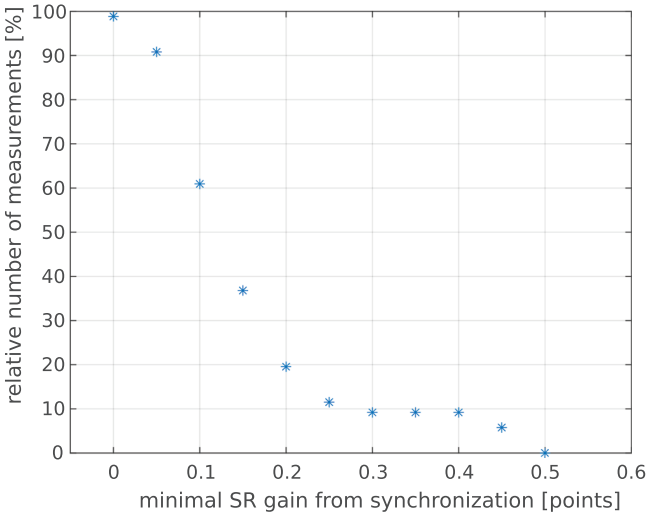

FIGURE 11 Success rate gain from synchronization across all considered measurements

4.4 | Impact of phase angle information/synchronization

In the previous part, we showed that the synchronization of the measurements could reduce by a factor of up to 2 the impact of misestimation of line impedance values (considering no synchronization errors); however, it appears that this impact is not

uniform across the measurement positions. When looking at all 87 considered measurements across the 20 reconstructed feeders, only the measurements placed at the most remote nodes in the longest feeders have shown an important potential maximal gain in SR with synchronization (considering no synchronization errors). We compared the success rate using synchronized and unsychronized data on all measurement locations. The difference of success rate is called success rate gain. Figure 11 shows how many of the considered measurement locations present a gain superior to a given value. We observe a flat curve from 0.25 SR gain up to 0.4 SR gain, meaning that around 10% of the measurements highly benefit from synchronization with a SR rate rising by up to 40 points for all of them. This reinforces the viability of the FLM, given that we are able to provide a DSO with a map showing the measurement nodes where investing in PMUs is most profitable.

5 | CONCLUSION

This paper presents a fault location method which has been developed specifically for MV distribution feeders. Simulations show promising locating potential with a rather small number of added measurement nodes. This paper shows that this method leverages synchronization at multiple levels, which support the increasing deployment of PMUs in the distribution grids. Since this algorithm is based on zero-sequence components, the location is not sensitive to the presence and variations of distributed generation (DG) currents as long as there is an isolation transformer with one of its windings being delta-coupled, which is the most common case in French MV networks. Moreover, it has proven to be robust to variations of fault impedance values (which can be high in distribution grids) and estimation errors in the values of zero-sequence capacitances, but it is sensitive to the estimation of line series resistances and reactances. With respect to [24], an optimal placement algorithm has been developed which quantifies the priority of the remote end substations for instrumentation. This would enable DSOs to select the best nodes for fault location for a given number of additional measurements while having an impact on the location precision as low as possible. Still remains the need to quantify the real gains that can be obtained considering synchronized measurement with synchronisation errors. To further enhance the performances of this FLM, an extrapolation of the two voltage estimates could be performed on virtual nodes around the projection node in weakly ramified feeders to obtain a smaller solution area. Moreover, this paper shows that the coupling between this method and already deployed impedance-based ones bears a great potential. Besides, on highly ramified feeders, there is a need for a robust version of the fault location method since one measurement can easily wrongly estimate the projection node in real conditions with the showed uncertainties, especially measurement errors. Since the length of the solution area Ω_{sol}^{M-1} can be very high with respect to the length of Ω_{sol}^{M}, selecting Ω_{sol}^{M-1} as solution area to improve robustness might mean enlarging the length of the solution by a high factor. Besides, it appears that, most of the time, the wrongly estimated projection nodes lie in the close neighbourhood of the real one. That is why a robust method should be investigated and designed based on a trade-off between enlargement of the fault location area and improvement of the robustness.

AUTHOR CONTRIBUTIONS

Alexandre BACH: Conceptualization, data curation, formal analysis, investigation, methodology, resources, software, supervision, validation, visualization, writing - original draft. Trung Dung Le: Conceptualization, formal analysis, methodology, supervision, writing - review and editing. Marc Petit: Formal analysis, funding acquisition, project administration, supervision, writing - review and editing.

CONFLICT OF INTEREST

The authors have declared no conflict of interest.

DATA AVAILABILITY STATEMENT

Research data are not shared.

ORCID

Alexandre Bach https://orcid.org/0000-0003-3706-3454
Trung Dung Le https://orcid.org/0000-0001-9959-0925

REFERENCES

1. Stefanidou-Voziki, P., Sapountzoglou, N., Raison, B., Dominguez-Garcia, J.: A review of fault location and classification methods in distribution grids. Electr. Power Syst. Res. 209, 108031 (2022)
2. VENTEEA. Smart Grids - Le site édité par la CRE. https://www.smartgrids-cre.fr/projets/venteea (visited on 06/02/2022).
3. Krishnathevar, R., Ngu, E.E.: Generalized impedance-based fault location for distribution systems. IEEE Trans. Power Delivery 27(1), 449–451 (2012)
4. Dashti, R., Ghasemi, M., Daisy, M.: Fault location in power distribution network with presence of distributed generation resources using impedance based method and applying π line model. Energy 159, 344–360 (2018)
5. Apostolopoulos, C.A., Arsoniadis, C.G., Georgilakis, P.S., Nikolaidis, V.C.: Fault location algorithms for active distribution systems utilizing two-point synchronized or unsynchronized measurements. Sustainable Energy, Grids and Networks 32, 100798 (2022)
6. Le, T., Petit, M.: Earth fault location based on a modified takagi method for MV distribution networks. In: 2016 IEEE International Energy Conference (ENERGYCON), pp. 1–6. IEEE, Piscataway, NJ (2016)
7. Liao, Y.: Fault location for single-circuit line based on bus-impedance matrix utilizing voltage measurements. IEEE Trans. Power Delivery 23(2), 609–617 (2008)
8. Schweitzer, E.O., Guzmán, A., Mynam, M.V., Skendzic, V., Kasztenny, B., Marx, S.: Locating faults by the traveling waves they launch. In: 2014 67th Annual Conference for Protective Relay Engineers, pp. 95–110. IEEE, Piscataway, NJ (2014)
9. Qiao, J., Yin, X., Wang, Y., Xu, W., Tan, L.: A multi-terminal traveling wave fault location method for active distribution network based on residual clustering. Int. J. Electr. Power Energy Syst. 131, 107070 (2021)
10. He, S., Cozza, A., Xie, Y.-Z.: Electromagnetic time reversal as a correlation estimator: Improved metrics and design criteria for fault location in power grids. IEEE Trans. Electromagn. Compat. 62(2) 598–611 (2020)
11. Wang, Z., Razzaghi, R., Paolone, M., Rachidi, F.: Electromagnetic time reversal similarity characteristics and its application to locating faults in power networks. IEEE Trans. Power Delivery 35(4), 1735–1748 (2020)

12. Magnago, F.H., Abur, A.: Fault location using wavelets. IEEE Trans. Power Delivery 13(4), 1475–1480 (1998)
13. Chen, K., Hu, J., Zhang, Y., Yu, Z., He, J.: Fault location in power distribution systems via deep graph convolutional networks. IEEE J. Sel. Areas Commun. 38(1), 119–131 (2020)
14. Srivastava, A., Parida, S.: A robust fault detection and location prediction module using support vector machine and gaussian process regression for AC microgrid. IEEE Trans. Ind. Appl. 58(1) 930–939 (2022)
15. Li, J.-M., Chu, S.-C., Shao, X., Pan, J.-S.: A single-phase-to-ground fault location method based on convolutional deep belief network. Electr. Power Syst. Res. 209, 108044 (2022)
16. Garcia-Santander, L., Bastard, P., Petit, M., Gal, I., Lopez, E., Opazo, H.: Down-conductor fault detection and location via a voltage based method for radial distribution networks. IEE Proc. Gener. Transm. Distrib. 152(2), 180–184 (2005)
17. Jamali, S., Bahmanyar, A.: A new fault location method for distribution networks using sparse measurements. Int. J. Electr. Power Energy Syst. 81, 459–468 (2016)
18. Mazlumi, K., Abyaneh, H.A., Sadeghi, S.H.H., Geramian, S.S.: Determination of optimal PMU placement for fault-location observability. In: 2008 Third International Conference on Electric Utility Deregulation and Restructuring and Power Technologies, pp. 1938–1942. IEEE, Piscataway, NJ (2008)
19. Nuqui, R.F., Phadke, A.G.: Phasor measurement unit placement techniques for complete and incomplete observability. IEEE Trans. Power Delivery 20(4), 2381–2388 (2005)
20. Liao, Y.: Fault location observability analysis and optimal meter placement based on voltage measurements. Electr. Power Syst. Res. 79(7), 1062–1068 (2009)
21. Silveira, E.G., Pereira, C.: Transmission line fault location using two-terminal data without time synchronization. IEEE Trans. Power Syst. 22(1), 498–499 (2007)
22. Gong, Y., Mynam, M., Guzman, A., Benmouyal, G., Shulim, B.: Automated fault location system for nonhomogeneous transmission networks. In: 2012 65th Annual Conference for Protective Relay Engineers, pp. 374–381. IEEE, College Station, TX (2012)
23. Teninge, A., Pajot, C., Raison, B., Picault, D.: Voltage profile analysis for fault distance estimation in distribution network. In: 2015 IEEE Eindhoven PowerTech, pp. 1–5. IEEE, Piscataway, NJ (2015)
24. Buzo, R.F., Barradas, H.M., Leão, F.B.: A new method for fault location in distribution networks based on voltage sag measurements. IEEE Trans. Power Delivery 36(2), 651–662 (2021)
25. Crespo, D.L.C.: New technique for fault location in distribution systems using sincrophasor voltages. Electr. Power Syst. Res. 212, 108485 (2022)
26. Bach, A., Le, T.-D., Petit, M.: A zero-sequence impedance-based fault location method for MV distribution feeders with sparse measurements. In: 16th International Conference on Developments in Power System Protection (DPSP 2022). IET Digital Library, Newcastle, UK, pp. 7–12.
27. Venegas, F.G.: Electric vehicle integration into distribution systems: Considerations of user behavior and frameworks for flexibility implementation. PhD thesis, Université Paris-Saclay (2021).
28. STE EDF GDF services. B6121_principes_protection.pdf. (Feb. 1, 1994).

How to cite this article: Bach, A., Le, T.D., Petit, M.: Sensitivity assessment of a novel earth fault location method with optimally placed distributed measurements for MV networks. IET Gener. Transm. Distrib. 17, 1358–1367 (2023). https://doi.org/10.1049/gtd2.12740